https://doi.org/10.5194/wcd-2021-63
Preprint. Discussion started: 4 October 2021

Weather and Climate Dynamics Discussions
Open Access

Strengthening tropical influence on heat generating circulation over Australia through spring

Roseanna C. McKay[1,2,4], Julie M. Arblaster[1,2,3], Pandora Hope[4]

[1] School of Earth, Atmosphere and Environment, Monash University, Victoria, Australia
[2] Australian Research Council Centre of Excellence for Climate Extremes
[3] National Center for Atmospheric Research, Boulder, Colorado, U.S.A.
[4] Bureau of Meteorology, Melbourne, Victoria, Australia
Correspondence to: Roseanna C. McKay (roseanna.mckay@bom.gov.au

Abstract

Extreme maximum temperatures during Australian spring can have deleterious impacts on a range of sectors from health to wine grapes to planning for wildfires, but are relatively understudied compared to spring rainfall. Spring maximum temperatures in Australia have been rising over recent decades, and, as such, it is important to understand how Australian spring maximum temperatures develop. Australia's climate is influenced by variability in the tropics and extratropics, but some of this influence impacts Australia differently from winter to summer, and, consequently, may have different impacts on Australia as spring evolves. Using linear regression analysis, this paper explores the atmospheric dynamics and remote drivers of high maximum temperatures over the individual months of spring. We find that the drivers of early spring maximum temperatures in Australia are more closely related to low-level wind changes, which in turn are more related to the Southern Annular Mode than variability in the tropics. By late spring, Australia's maximum temperatures are proportionally more related to warming through subsidence than low-level wind changes, and more closely related to tropical variability. This increased relationship with the tropical variability is linked with the breakdown of the subtropical jet through spring and an associated change in tropically-forced Rossby wave teleconnections. However, much of the maximum temperature variability cannot be explained by either tropical or extratropical variability. An improved understanding of how the extratropics and tropics projects onto the mechanisms that drive high maximum temperatures through spring may lead to improved sub-seasonal prediction of high temperatures in the future.

https://doi.org/10.5194/wcd-2021-63
Preprint. Discussion started: 4 October 2021

1. Introduction

Anomalously high Australian spring (September-October-November) maximum temperatures can be highly impactful. High temperatures may negatively impact health due to a lack of acclimatisation (e.g. Nairn and Fawcett, 2014), and agriculture by changing growing season length and crop yields (Cullen et al., 2009; Jarvis et al., 2019; Taylor et al., 2018). Hotter and drier spring conditions have been linked to an earlier start to (Dowdy, 2018) and preconditioning of (Abram et al., 2021) the summer fire season. The trend toward higher temperatures over recent decades (Collins et al., 2013), means that anomalous high maximum temperatures may occur more often (e.g. Alexander and Arblaster, 2009). Several recent springs have already exceeded historic temperature records, with some spring months breaking records that were set only the previous year (Arblaster et al., 2014; Gallant and Lewis, 2016; Hope et al., 2015; McKay et al., 2021). Much of this observed anomalous heat has been attributed to the background global warming trend (Arblaster et al., 2014; Gallant and Lewis, 2016; Hope et al., 2015; Hope et al. 2016). However, gaps remain in our understanding of what drives anomalous high maximum temperatures in Australia during spring, and particularly on the monthly time-scale that some of these heat events occurred over. As the globe continues to warm, a better understanding of what makes a spring month in Australia hot today will lead to greater resilience against extreme heat in the future.

High spring temperatures have been linked with several remote modes of variability in the tropics and extratropics. In the tropics, the positive phases of El Niño Southern Oscillation (ENSO) in the tropical Pacific and the Indian Ocean Dipole (IOD) in the tropical Indian Ocean are the strongest drivers of high maximum temperatures in Australia in spring, particularly in the south and east (Power et al., 1998; Jones and Trewin, 2000; Saji et al., 2005; Min et al., 2013; White et al., 2014). Many more studies focus on the ENSO and IOD relationships to drier spring conditions (Nicholls et al., 1989; Meyers et al., 2007; Ummenhofer et al., 2009; Risbey et al., 2009a; Watterson, 2010; Cai et al., 2011; Min et al., 2013; Pepler et al., 2014; McIntosh and Hendon, 2018; Watterson, 2020) and to more extreme spring fire weather (Harris and Lucas 2019; Marshall et al. 2021). While ENSO and the IOD co-vary significantly in austral spring (e.g. Meyers et al., 2007), they can occur independently (e.g.

https://doi.org/10.5194/wcd-2021-63
Preprint. Discussion started: 4 October 2021

Risbey et al 2009a). Further, the IOD's influence on Australia's temperature peaks around SON (Saji et al., 2005) compared to around NDJ (November-December-January) for ENSO (Jones and Trewin, 2000). It can be useful to look at a single index that describes the large-scale tropical SST variability's influence on Australia, such as the tropical tripole index (TPI) (Timbal and Hendon, 2011). While other tropical modes of variability, such as the Madden-Julian Oscillation (MJO), also influence Australia's spring maximum temperatures (e.g. Wheeler and Hendon, 2004; Wheeler et al., 2009; Marshall et al., 2014), we focus on the tropical SST-driven influence on Australia's spring climate.

Variability in the extratropics is also linked to high temperatures in Australia. The negative phase of the Southern Annular Mode (SAM), the primary mode of variability in the extratropics, (Hendon 2007; Risbey et al., 2009a; Min et al., 2013; Marshall et al., 2012, Hendon et al., 2014; Fogt and Marshall, 2020**)** drives hotter and drier Australian spring conditions, and to more extreme spring fire weather (Marshall et al. 2021). SAM generally varies at a higher frequency than ENSO or the IOD, however, SAM also has lower frequency variations. On a seasonal timescale, El Niño promotes negative SAM, particularly during the warmer months (L'Heureux and Thompson, 2006; Hendon et al., 2007; Lim et al., 2016; Lim et al., 2019a). Polar stratospheric weakening during austral spring (sometimes associated with sudden stratospheric warming) can also sustain negative SAM (Lim et al., 2018)) and higher Australian maximum temperatures from late spring (Lim et al., 2019b). As with ENSO and the IOD, more studies focus on how SAM influences Australian rainfall than temperature, particularly when examining the teleconnection pathway. While low rainfall correlates well with high maximum temperatures (Simmonds, 1998; Jones and Trewin, 2000; Timbal et al., 2002; Hope and Watterson, 2018), there is a gap in our understanding of how both tropical and extratropical modes of variability impact spring maximum temperature.

Anomalously high geopotential height (or, synonymously, anticyclonic vorticity) over southern Australia is associated with spring high maximum temperatures in Australia (Hope et al., 2015**;** Gallant and Lewis 2016; McKay et al., 2021). While ENSO, the IOD, and the tropical TPI also promote anomalously high geopotential height, it forms further to the south of Australia (e.g. Cai et al., 2011; Timbal and Hendon, 2011; McIntosh and Hendon,

https://doi.org/10.5194/wcd-2021-63
Preprint. Discussion started: 4 October 2021

2018). SAM's negative phase is characterised by an equatorward shift of the eddy-driven jet and bands of anomalously low and high geopotential height in the mid- and high-latitudes respectively (Thompson and Wallace, 2000; Fogt and Marshall, 2020). The altered atmospheric flow associated with the drivers can reduce rainfall, including by defecting cooling rain-bearing systems (e.g. Jones and Trewin 2000; Hendon et al., 2007; Pepler et al., 2014; van Rensch et al., 2019) away from Australia (Cai et al., 2011; Risbey et al., 2009b; McIntosh and Hendon, 2018; Hauser et al., 2020). Anomalous heat and dry is also associated with other mechanisms such as increased subsidence and insolation (Hendon et al., 2014; Lim et al., 2019b; Pfahl et al., 2015; Quinting and Reeder, 2017; Suarez-Gutierrez et al., 2020) or heat advection (Jones and Trewin, 2000; Boschat et al., 2015; Gibson et al., 2017). Understanding the differences between the extratropical and tropical forcing behind some of these heat mechanisms is a goal of this paper.

The mechanisms and atmospheric circulation patterns associated with heat and connections to remote drivers may also vary through spring. McKay et al. (2021) noted that the relationship with the southern Australian upper-anticyclone and maximum temperature is weaker in September than November, and suggested that the anticyclone had greater influence from the tropics in later spring. The impact of SAM in the extratropics on Australia's temperature reverses from winter to spring (Hendon et al., 2007; Risbey et al., 2009a; Marshall et al., 2012; Min et al., 2013; Hendon et al., 2014; Fogt et al., 2020) as the mean zonal winds change with the seasons (Hendon et al. 2007) and the Indo-Pacific subtropical jet (STJ) weakens (Bals-Elsholz et al., 2001; Koch et al., 2006; Ceppi and Hartmann, 2013, Gillett et al., 2021) so that a negative SAM phase enhances subsidence over subtropical Australia into the warmer months (Hendon et al., 2014). The IOD and ENSO teleconnection pathways over the Indian Ocean toward Australia also change from winter to spring (Cai et al., 2011). This change may relate to the strength of the winter STJ, as it should prevent direct propagation of Rossby waves between the tropics and extratropics (e.g. Hoskins and Ambrizzi, 1993). McIntosh and Hendon (2018) proposed that transient eddy-feedbacks generate a secondary wave source south of the winter STJ in response to IOD forcing. In spring, the STJ weakens sufficiently to allow for direct Rossby wave propagation from the tropical Indian Ocean. However, McKay et al. (2021) suggested that

https://doi.org/10.5194/wcd-2021-63
Preprint. Discussion started: 4 October 2021

the STJ may not weaken sufficiently in September to allow direct Rossby wave propagation, and that teleconnection pathways may be different on a monthly timescale as a result.

Teleconnections driven by large-scale remote modes of variability can precondition Australia toward hotter and spring conditions (e.g. Hurrell et al., 2009), but cannot guarantee a hot month or season will eventuate. Even the strongest El Niño events may not result in the canonical dry and warm conditions expected (van Rensch et al., 2019; Hauser et al., 2020). Further, differences in how those modes of variability influence Australia between winter-spring-summer and the differences between spring-average atmospheric circulation highlight that there is more to understand in how maximum temperatures evolve through spring months. Filling the gap between weather and seasonal time-scales is an ongoing area of research that can lead to improved sub-seasonal forecasting (Meehl et al., 2021). Given the increasing likelihood of future extreme heat events occurring through spring, it is imperative to understand any differences that may exist in how heat develops, and links to varying influences from the extratropics to tropics. The reanalysis datasets, Rossby wave and statistical analysis methods are described in Section 2. An overview of how Australian spring maximum temperatures are related to circulation and large-scale variability is in Section 3. In Section 4 the variation of these relationships through the months of spring are assessed and Section 5 describes how the drivers influence the mechanisms that promote high monthly maximum temperature. Discussion and conclusions are provided in Section 6

2. Methods and data

2.1 Indices and datasets

All circulation variables for September, October, November monthly-averaged data are taken from the ECMWF's Reanalysis 5 (ERA5) (Hersbach et al., 2020) available from the Copernicus Climate Change Service (C3S, 2017) on a 0.25° grid from 1979 to 2019. Low-level circulation is diagnosed using 850hPa horizontal wind and mean sea level pressure (MSLP). Mid-tropospheric vertical motion is represented by 500hPa omega. Upper-level circulation is represented by 200hPa geopotential height (200Z). 200hPa horizontal winds are used for

https://doi.org/10.5194/wcd-2021-63
Preprint. Discussion started: 4 October 2021

Rossby wave analysis. Similar results were found using ERA-Interim reanalysis (Dee et al, 2011) and the JRA-55 from the Japan Meteorological Agency (2013) (not shown).

Australian monthly-averaged daily maximum temperature data for 1979 to 2019 is taken from the Australian Water Availability Project (AWAP) (Jones et al., 2009) analyses, available on a 0.05° resolution grid.

Monthly sea surface temperature (SST) is taken from NOAA Extended Reconstructed Sea Surface Temperature (ERRSST V5; Huang et al., 2017)

The impacts of SAM on Australia's climate shows some sensitivity to the method used to calculate the SAM index (e.g. Risbey et al., 2009a). To ensure consistency between the other indices and circulation variables, we calculate SAM as the difference between the standardized zonal means of ERA5 MSLP anomalies at 60°S and 40°S (Gong and Wang, 1999).

The tropical TPI (Timbal and Hendon, 2011) is defined as the difference in SST averaged over a parallelogram located over the Maritime Continent (0°-20S, 90°-140E at the equator shifted to 110°-160°E at 20°S) from SST averaged and summed over two regions in the tropical Indian Ocean (10°N to 20°S, 55° to 90°E) and tropical Pacific Ocean (a trapezium that extends from 15°N to 15°S, 150°E to 140°W in the north and 180°E to 140°W in the south). ENSO is described using the Niño3.4 index (averaged SST anomalies over 5°N-5°S, 170°E-120°W) and the IOD using the dipole mode index (DMI; the difference between the SST anomalies averaged over 10°S-10°N, 50°-70°E and 10°S-0°, 90°-110°E; Saji et al., 1999).

To highlight the influence of interannual variability, the 1981-2010 climatological mean is removed from each month, and the data is linearly detrended before analysis.

https://doi.org/10.5194/wcd-2021-63
Preprint. Discussion started: 4 October 2021

2.3 Rossby wave analysis

We use wave activity flux (WAF) at 200hPa to trace Rossby wave group propagation and to identify source and decay regions that influence the atmospheric circulation patterns. Following Takaya and Nakamura (2001), we calculate WAF as:

$$WAF = pcos\phi\left\{\frac{U}{a^2cos^2\phi}\left[\left(\frac{\partial\psi'}{\partial\lambda}\right)^2 - \psi'\frac{\partial^2\psi'}{\partial\lambda^2}\right]\right.$$

$$+\frac{V}{a^2cos\phi}\left[\frac{\partial\psi'}{\partial\lambda}\frac{\partial\psi'}{\partial\phi} - \psi'\frac{\partial^2\psi'}{\partial\lambda\partial\phi}\right] \frac{U}{a^2cos\phi}\left[\frac{\partial\psi'}{\partial\lambda}\frac{\partial\psi'}{\partial\phi} - \psi'\frac{\partial^2\psi'}{\partial\lambda\partial\phi}\right]$$

$$\left.+\frac{V}{a^2}\left[\left(\frac{\partial\psi'}{\partial\phi}\right)^2 - \psi'\frac{\partial^2\psi'}{\partial\phi^2}\right]\right\}$$

where p is the pressure (200hPa) scaled against 1000hPa, U and V are the climatological zonal and meridional wind speed magnitudes, a is the radius of the earth, (ϕ, λ) are latitude and longitude, $\psi' = Z'/f$ is the quasi-geostrophic perturbation streamfunction, Z' is the 200hPa geopotential height anomaly obtained through regression onto maximum temperature or climate driver indices, $f = 2\Omega sin\phi$ is the Coriolis parameter with the Earth's rotation Ω. WAF is not plotted within 10° of the equator.

WAF propagates in the direction of quasi-stationary Rossby wave group velocity, and regions of divergence or convergence of WAF correspond to zones of Rossby wave sources or sinks respectively.

Total stationary Rossby wave wavenumber (e.g., Hoskins and Karoly 1981) **is** defined as:

$$K_S = \sqrt{\frac{\beta - U_{yy}}{U}}$$

where $\beta - U_{yy}$ is the meridional gradient of mean-state absolute vorticity at 200hPa. WAF should refract toward regions of higher K_S and either reflect or evanesce on regions of K_S<0, such as in the STJ where the curvature of the flow (U_{yy}) can become larger than the planetary vorticity gradient (β) (e.g Barnes and Hartmann, 2012; Li et al., 2015 a,b)

https://doi.org/10.5194/wcd-2021-63
Preprint. Discussion started: 4 October 2021

Weather and Climate Dynamics Discussions
Open Access
EGU

2.4 Statistical analysis

Linear, partial, and multi-linear regression and Spearman's ranked correlation are used to assess the relationships between Australian maximum temperature, atmospheric circulation and the tropics and extratropics. Due to the large decorrelation length scales, Australian-average maximum temperature variability is representative of all but far north Australia's spring and spring-monthly maximum temperatures (Sup. Fig. 1). Statistical significance is calculated at the 95% confidence level using Student's (1908) t-test using 39 (41 years - 2) degrees of freedom. Pattern correlation is used to compare regression patterns.

3. Spring-season maximum temperatures - circulation patterns and associations with drivers

We start by giving an overview of the spring-seasonal relationships between average Australian austral spring maximum temperature and lower- and upper-level atmospheric circulation (Fig 1a,b). Barotropic cyclones appear to the southwest and southeast of Australia, occurring in both the lower- and upper-level circulation regressions (Fig. 1a-b) and noted during recent extreme spring heat events (Gallant and Lewis, 2016; Hope et al., 2016; McKay et al., 2021). Weak anticyclonic low-level winds are found over Australia, as well as sinking motion across the eastern half of the continent. An upper-level anticyclone sits over southern Australia, with the wave activity flux predominantly propagating from the subtropical Indian Ocean, through the anticyclone and into the subtropical Pacific Ocean.

We now compare the atmospheric patters associated with spring maximum temperature to those associated with large scale modes of variability. The spring-average atmospheric circulation patterns associated with the remote drivers of variability are calculated via linear regression onto each standardised index. Note that the TPI and SAM indices have been multiplied by negative one to present positive associations with high temperatures. The pattern for SAM (x-1) shows elongated barotropic low and high anomalies lie in the middle and high latitudes respectively (Fig. 1c-d), with upper-level cyclonic nodes to the southeast

https://doi.org/10.5194/wcd-2021-63
Preprint. Discussion started: 4 October 2021

and southwest of Australia. Negative SAM is associated with high maximum temperatures through much of subtropical, and particularly eastern, Australia (Fig. 1e).

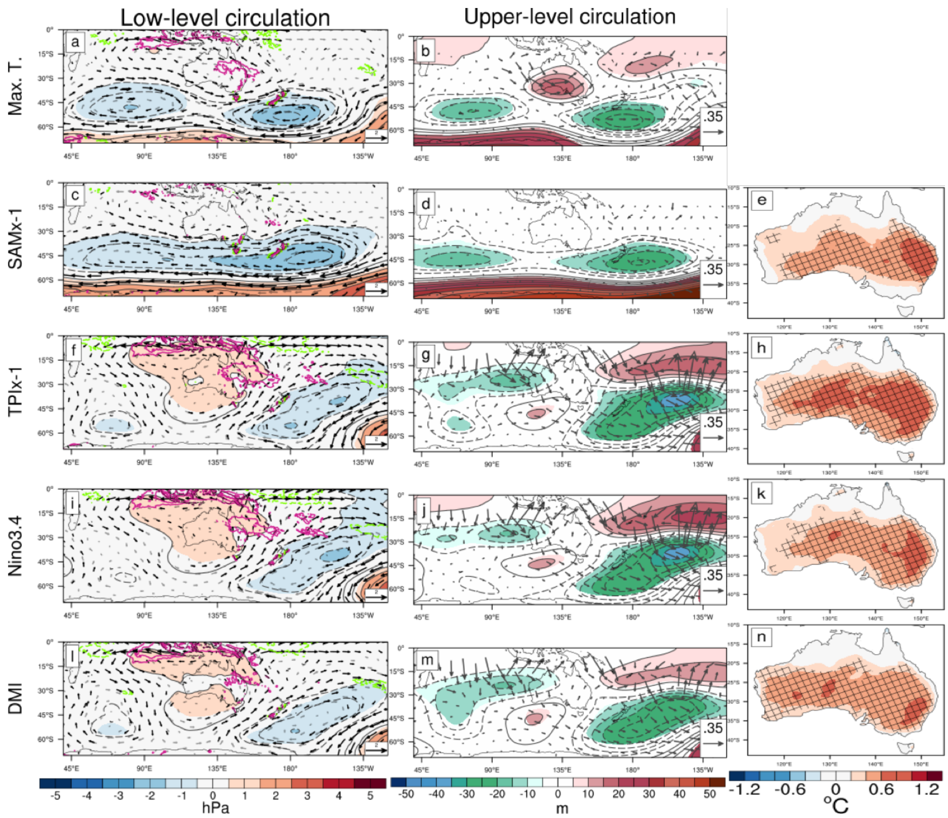

Figure 1. Linear regressions of spring standardised weighted area-averaged Australian maximum temperature (a-b), SAMx-1 (c-e), tropical TPIx-1 (f-h), Niño3.4 (i-j) and DMI (j-n) onto low-level circulation (left column), upper-level circulation (middle column) and Australian maximum temperatures (right column). Low-level circulation is represented by anomalous mean sea level pressure (hPa) (black and filled contours), 850hPa wind vectors (ms^{-1}) and 500hPa omega ($hPas^{-1}$) contours from -0.02 to 0.02$hPas^{-1}$ in steps of 0.01 $hPas^{-1}$ (magenta contours are positive; downward motion) and cyan contours are negative; upward motion, and the zero contour is not plotted). Upper-level circulation is represented by 200hPa geopotential height (black and filled contours and wave activity flux vectors (m^2s^{-2}).
Filled contours, bold wind vectors, cross-hatching, and all vertical motion contours are significant at the 95% confidence level using a Student's t-test with 39 independent

The tropical modes, represented by Niño3.4 (Fig 1i-k), the DMI (Fig. 1 l-n), and tropical TPI (x-1) (Fig 1f-h)) are also associated with spring Australian maximum temperature anomalies. Each mode generates an apparent Rossby wave pattern that arcs from the tropical Indian

Ocean to promote anomalous high geopotential height south of Australia, consistent with earlier studies (e.g. Cai et al., 2011; Timbal and Hendon, 2011; McIntosh and Hendon, 2018). Each regression also shares anomalous high surface pressure over Australia, sinking motion in the east, cyclonic nodes to the southwest and east of Australia, and elongated upper-level cyclones in the subtropical Indian Ocean. These similarities are likely the result of the strong co-variability between the IOD and ENSO (e.g. Meyers et al., 2007; Risbey et al., 2009a). However, the IOD has a stronger low-level cyclone to the southeast and a poleward extension of the subtropical Indian Ocean cyclone that sets a subtly different wave train from around 50°S, 60°E that is poleward that generated by ENSO. The positive IOD is also associated with high maximum temperatures across a broader region of southern and western Australian than is El Niño. The tropical TPI (x-1) is a blend of both Niño3.4 and DMI circulation patterns and has a strong relationship with Australian spring maximum temperatures across all but northern Australia.

Given the similarities and connections between ENSO and IOD teleconnections, we use the tropical TPI to represent the large-scale influence of the tropics. SAM is used to represent the influence of the extratropics. Statistical models of Australian weighted area-averaged spring maximum temperatures reconstructed through multilinear regression using either Niño3.4, DMI and, SAM or the tropical TPI and SAM as the predictors explains 32% and 34% of maximum temperature variability respectively (sup. Fig. 2).

We next compare the atmospheric circulation associated with monthly high maximum temperatures to that with the large-scale modes of variability through the individual months of spring. To ensure that we are assessing the influence of the tropics and extratropics separately, we use multi-linear regression onto the monthly circulation variables.

4. Monthly circulation patterns and associations with drivers

The regression of monthly Australian maximum temperature onto the lower- and upper-level atmospheric circulation is displayed in Figures 2a-c and 3a-c respectively for September, October and November. The multi-linear regression onto the standardised monthly indices of SAM (x-1) (Figs. 2d-f and 3d-f) and tropical TPI (x-1) (Figs. 2h-j and 3h-j).

https://doi.org/10.5194/wcd-2021-63
Preprint. Discussion started: 4 October 2021

At first glance, these monthly circulation patterns are broadly similar to the spring-average regression patterns. However, the details of the circulation patterns change as the months progress, suggesting that different processes are important for heat development through spring.

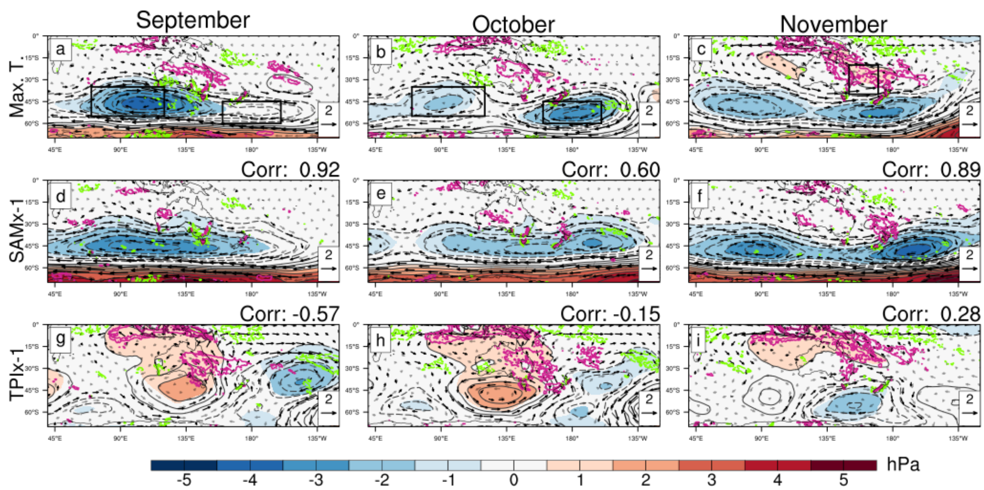

Figure 2. Regressions onto low-level circulation, as in Fig. 1, except for September (left column), October (middle column) and November (right column). Standardised areal-averaged Australian maximum temperature is linearly regressed onto low-level circulation (ta-c) and SAMx-1 (d-f) and tropical TPIx-1 (g-i) are multi-linear regressions onto low-level circulation.
Pattern correlation between the maximum temperature MSLP regressions and the SAM and tropical TPI regressions calculated over 5°S-70°S; 70°E-170°E are written in the top right of each SAM or tropical TPI regression.
The boxes (a-c) show key low-level circulation features identified as being important for maximum temperature development: The southwest cyclone (SWC) 35°S-55°S; 70°-120°E; southeast cyclone (SEC) 45°S-60°S; 160°-200°E and Tasman Sea high (TSH) 20°S-40°S; 150°-170°E

The most obvious change in atmospheric circulation through the months is in the low-level flow across Australia, particularly generated by the barotropic cyclones southwest (SWC) or southeast (SEC) of Australia (boxes in Fig 2a-b). Weak low-level anticyclonic flow around the Tasman Sea (box in Fig. 2c) also contributes to the northerly flow over eastern Australia in November in particular (Fig. 2c). Tasman Sea anticyclonic blocking patterns have previously

https://doi.org/10.5194/wcd-2021-63
Preprint. Discussion started: 4 October 2021

Weather and Climate Dynamics Discussions
Open Access
EGU

been linked to anomalously warm conditions (Marshall et al., 2014), but here appear to only contribute to high maximum temperatures in November. The SWC and SEC vary in geographic shape and strength through the months. The SWC dominates in September but weakens through October and November, whereas, the SEC is missing in September but is strong in October and November. Similar cyclones appear in the monthly SAM (x-1) regressions (Figs. 2 d-f, 3d-f) and the Australian-region MSLP correlates strongly with that associated with high Australian temperature (top-right of Fig 2d-f). Rather than cyclones in September and October the TPI (x-1) is associated with a barotropic anticyclone south of Australia that directs southerly low-level wind across eastern Australia (Figs. 2 h-j); a pattern that would be associated with cooler conditions. The September and October TPI (x-1) MSLP pattern actually anti-correlate with that associated with high Australian maximum temperatures (top-right Fig. 2 g-i). It is not until November that we see a barotropic cyclone to the southeast of Australia associated with the TPI (x-1). So, for the majority of spring negative TPI-forced low-level atmospheric circulation appears to counter high maximum temperatures, despite the overall positive relationship in spring (Fig. 1h).

The anomalous southern Australian upper-anticyclone (SAA) from the spring pattern appears is also associated with high maximum temperature in each of the individual spring months (Fig. 3a-c), but its location shifts eastward across Australia through spring. The boxed region was chosen to match earlier studies (Gallant and Lewis, 2016; McKay et al., 2021), but best matches the November position, likely contributing to the stronger relationship between heat and SAA in this month (McKay et al., 2021; see also section 6). The anticyclone in later spring appears to form part of a wave train from a cyclone to the northwest of Australia toward the southeast cyclone. While the monthly TPI regressions have anticyclones in September and October (Fig. 3g-h), they are located too far south relative to Australia, as in the spring-average regression. The regressions onto SAM (x-1) (Fig 3d-f) have weak anticyclones over western Australia that are not statistically significant. It is not until November that both SAM and TPI (x-1) (Figs 3 f, i) have an anticyclone over central-east southern Australia. Both the upper- level SAM and TPI (x-1) regressions correlate moderately with the maximum temperature regression in November, and the SAM and TPI (x-1) anticyclones may form part of the same wave train associated with maximum temperatures. However, the SAM and TPI (x-1) anticyclones are weaker and too far east

https://doi.org/10.5194/wcd-2021-63
Preprint. Discussion started: 4 October 2021

relative that associated with high maximum temperatures, such that they may not contribute strongly to the SAA formation. We explore this idea further in section 6.

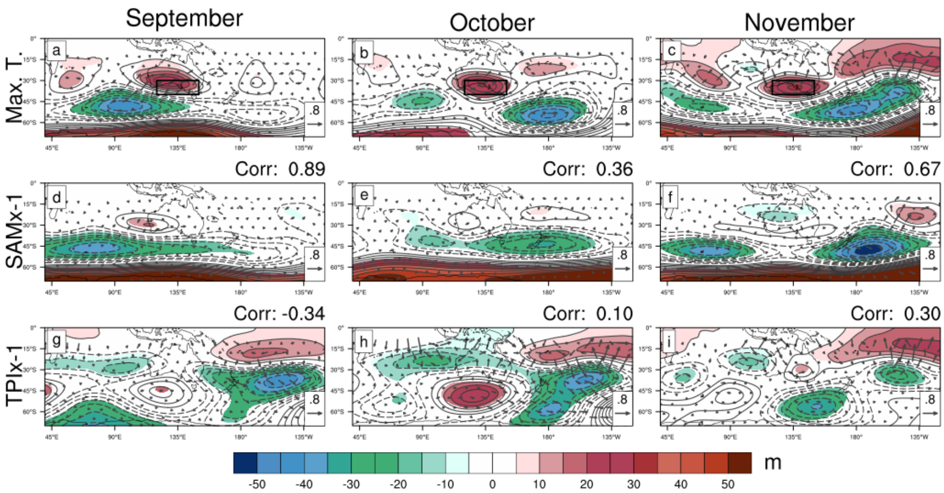

Figure 3. As with figure 2, but for upper-level circulation. The Australian-region pattern correlation between the maximum temperature Z200 regressions and SAMx-1 and TPIx-1 are in the top right of each figure. Boxed area (a-c) highlights the southern Australian anticyclone (SAA; 30°-40°S, 120°-150°E) that is linked with high maximum temperatures.

While the southern Australian anticyclone is not well explained by SAM or TPI (x-1) through spring, much of the statistically significant 500hPa vertical motion associated high maximum temperatures (green and magenta contours, Fig. 2a-c) matches that associated with TPI (Fig. 2h-j) and to a lesser extent SAM (Fig. 2d-f). In September, sinking motion over subtropical Australia and rising motion over the southern coasts is associated with high maximum temperatures. By November, the rising motion has largely vanished and the sinking motion has shifted to be over eastern Australia. It was expected that the SAA would generate some of the sinking motion associated with high maximum temperature, however, this vertical motion does not correlate strongly with any of the key circulation features examined here (Sup. Table1).

https://doi.org/10.5194/wcd-2021-63
Preprint. Discussion started: 4 October 2021

Changes in propagation of wave activity flux help explain some of the changes in the broad scale circulation changes through spring. In September, WAF predominantly propagates from the southwest cyclone toward the southern Australian anticyclone. In October, a component of WAF also propagates from the eastern tropical Indian Ocean region. By November, the tropical-component dominates the WAF and forms part of a very different pattern to the previous two months; continuous WAF propagates from the far southwest Indian Ocean, joins WAF propagating out of the tropical Indian Ocean and then continues across the southern Australian anticyclone. The latter part of this wave train is similar to the IOD teleconnection highlighted by Cai et al. (2011) in spring. The WAF associated with SAM and TPI (x-1) also propagates from the extratropics toward the respective anticyclones in September and October. While a broad region of low height in the subtropical Indian Ocean is associated with the TPI, it does not appear to generate WAF that propagates into the extratropics. It is not until November that WAF associated with the TPI (x-1), and weakly with SAM (x-1), appears to propagate directly from the cyclone in the eastern subtropical Indian Ocean through the anticyclone over southeastern Australia.

Overall, these results suggest that the circulation associated with maximum temperature shifts from extratropical to tropical forcing as spring progresses. This is supported by how well SAM appears to project onto the atmospheric circulation associated with maximum temperatures in September, and how the TPI projects more strongly later in spring. The change in WAF associated with this change suggests that there may be a blocking mechanism between the tropics and extratropics generating this change.

We find qualitatively similar results if we perform the linear regressions using maximum temperature averaged over sub-regions of Australia, for example southwest or southeast Australia (Supplemental Fig S2).

5. Connection between subtropical jet and atmospheric circulation

We next explore how the subtropical jet may be influencing the WAF through the spring months.

https://doi.org/10.5194/wcd-2021-63
Preprint. Discussion started: 4 October 2021

The subtropical jet (STJ) peaks in strength in winter and weakens through spring to have broken down by summer (e.g. see figure 9, Ceppi and Hartmann, 2013). This gradual breakdown of the STJ coincides with a decrease in the area with total stationary wavenumber less than zero over southern Australia (Fig. 4), and may provide an explanation for the growing relationship with the tropics and Australian maximum temperature by November.

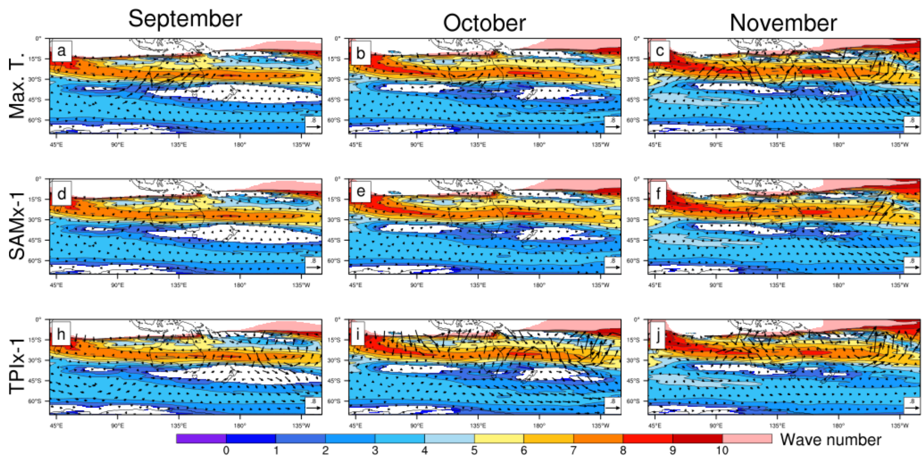

Figure 4. Total wave number (K) calculated for September, October and November. Vectors are the wave activity flux repeated from figure 3.

The wave activity flux vectors from the maximum temperature, TPI and SAM (x-1) regressions in figure 3 are overlaid in figure 4 on the monthly climatological Ks associated with the zonal winds. In September, the WAF associated with high maximum temperature (Fig. 4a) diverges from the region of the southwest cyclone to propagate through a region of low total stationary Rossby wave wavenumber, Ks, over southwest Australia and along the STJ waveguide (i.e. from high to low latitudes). As the jet weakens in October (Fig. 4b) a portion of WAF also diverges from the tropical Indian Ocean to dissipate on the jet's equatorward flank, but mostly propagates from west to east along the STJ waveguide. Even more distinctive, by November (Fig 4c), WAF propagates along the jet waveguide to a region near Africa, with contributions from the tropical Indian Ocean, but does not appear to propagate out of the SWC.

The increase in WAF associated with the tropical TPI (Fig 4h-j) propagating out of the tropical Indian Ocean through spring appears to coincide with the STJ decay. In September

https://doi.org/10.5194/wcd-2021-63
Preprint. Discussion started: 4 October 2021

and October weak WAF diverging from the central southern Indian Ocean follows the eddy-driven jet waveguide (region of locally higher wave number around 50°S), suggesting the secondary wave source proposed by McIntosh and Hendon (2018) is important in early spring. The tendency for TPI-associated WAF to form and follow this trajectory may explain why the barotropic anticyclone associated with the TPI is further poleward than in the regression onto Australian maximum temperature. By October more WAF is propagating out of the tropical Indian Ocean along the region of high Ks and by November WAF is propagating out of the extratropical Indian Ocean along the high Ks region, similar to the maximum temperature-WAF. WAF generated by SAM (Fig. 4d-f) also converges toward the STJ waveguide in each month.

Limits around linear Rossby wave theory (e.g. Liu & Alexander, 2007) may explain why some wave activity flux cross the region of imaginary wavenumber associated with the STJ. However, the majority of WAF associated with Australian maximum temperature, or with the tropics or extratropics does divert to propagate along the jet, as expected. While the breakdown of the STJ through spring may help explain the change in teleconnection pathways of the TPI toward Australia, the STJ consistently acts as a waveguide toward Australia.

We now look more closely into how the drivers, circulation features, and heat mechanisms relate to each other and how that results in higher Australian maximum temperatures.

6. Mechanisms and drivers of monthly maximum temperatures through spring

As with the atmospheric circulation regressions, the relationships between Australian maximum temperature and SAM and TPI (x-1) evolve through the spring months. In September, negative SAM (Fig. 5a) is associated with a broad area of high maximum temperature over subtropical Australia, that contracts in October and November (Figs. 5 b-c). Conversely, the relationship with negative TPI and maximum temperature is weaker early in spring, with statistically significant high temperatures confined to the west and east, and cool temperatures in the far north in September (Fig. 5d). The TPI’s relationship with high maximum temperature broadens and strengthens in October and covers the majority of

https://doi.org/10.5194/wcd-2021-63
Preprint. Discussion started: 4 October 2021

Australia by November (Figs. 5 e-f). Overall, these monthly relationships give the impression of a transition from extratropical to tropical drivers becoming more influential over Australian temperatures that is broadly consistent with the apparent change in atmospheric circulation through spring.

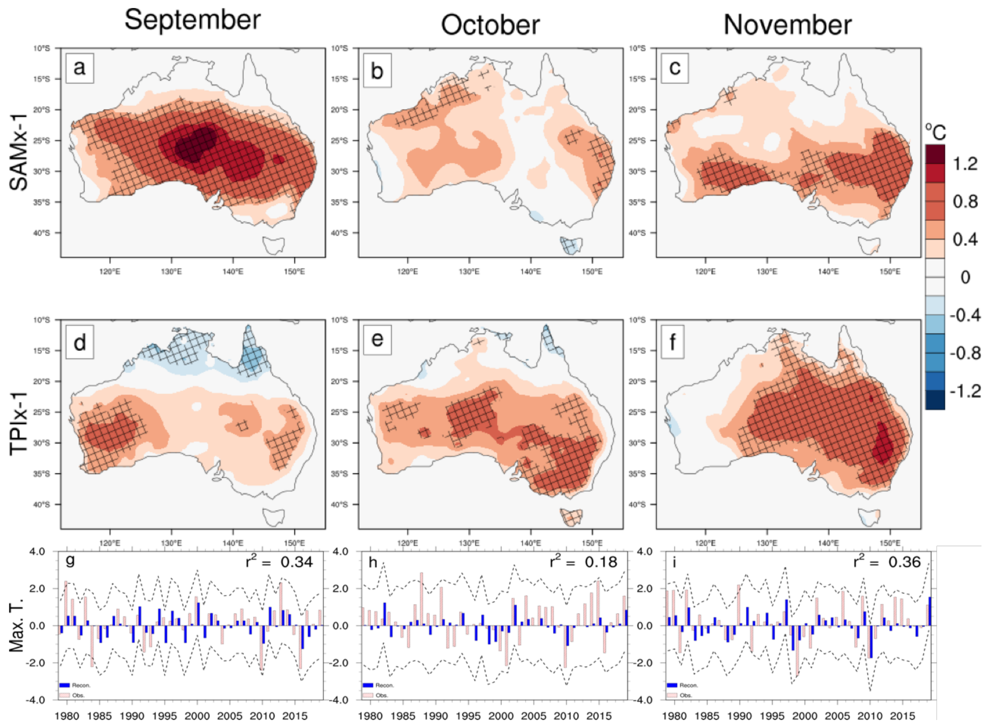

Figure 5. Multilinear regression coefficients (°C) of Australian maximum temperature regressed onto standardised timeseries of the SAMx-1 (a –c) and the tropical TPI x-1 (d - f) for September, October and November over the years 1979 to 2019. Reconstructions (blue bars) of September, October and November (i-k) Australian area-averaged maximum temperature from standardised time series of SAM and tropical TPI indices. Observed values are in blue. The dashed line shows the 95% prediction interval computed as +/-1.96 standard error and the variance explained (r^2) of the model is in the top right of each figure.

Using the standardised SAM and TPI time series as predictors in a regression model to reconstruct the monthly Australian-averaged maximum temperature anomalies (Figs 4g-i) explains only between 18 and 36% Australian maximum temperature variance (r^2) through spring. The model does not substantially improve if it is calculated over southeast or southwest Australia, or if using Niño3.4 or DMI as predictors instead of the tropical TPI (Sup. Fig.4).

https://doi.org/10.5194/wcd-2021-63
Preprint. Discussion started: 4 October 2021

To explore how the atmospheric circulation relates to some of the mechanisms that develop heat through spring, we first compose indices of the key circulation features discussed in section 4. Weighted area-averages of mean-sea level pressure (multiplied by negative one) over the southwest and southeast cyclones (SWC and SEC) and 200hPa geopotential height over the southern Australian anticyclone (SAA) for each spring month. See Figs. 2a,b and 3a-c for regions. Creating a statistical model of Australian-averaged monthly spring maximum temperatures from these circulation features (Fig. 6a-c) explains consistently higher maximum temperature variance (around 60%) than did the model from the indices of tropical and extratropical large-scale modes of variability. Further, despite the changes in the features' geographic shape, strength and position across the spring months in Fig .2, the majority of maximum temperature across Australia is well explained by at least one of these features at all times through spring (Sup. Fig. 6). We next explore how these MSLP or 200hPa geopotential height features relate to the low-level westerly or northerly winds and vertical motion and how that relates to high maximum temperature development.

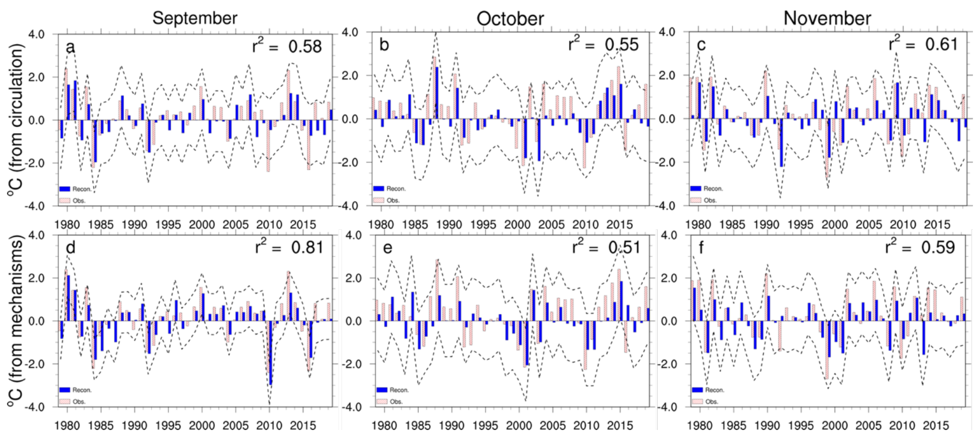

Figure 6. As in figure 4 (g-i), but using time series of key circulation features (south-west low, south-east low and southern Australian anticyclone) identified in figures 1 and 2 as predictors in the top row (a-c) and area-averaged dynamical heat mechanism components (850hPa zonal wind and meridional wind (multiplied by -1) and 500hPa vertical motion; see text for region averaged over) as predictors in the bottom row (d-e) for September, October, and November.

Following van Rensch et al (2019), indices of three dynamical heat mechanisms were created by weighted area-averaging of westerly and northerly wind (meridional wind multiplied by -1) over a region around southern Australia (25°S-45°S, 105°-155°E), and

https://doi.org/10.5194/wcd-2021-63
Preprint. Discussion started: 4 October 2021

500hPa vertical motion (omega; positive is sinking motion) averaged over subtropical Australia (15°S-25°S, 120°-155°E). Regions were selected based on the areas of highest statistical significance between atmospheric circulation and Australian maximum temperature in Fig. 2a-c. Again, a statistical model of Australian-averaged maximum temperatures that uses these mechanisms as the predictors explains a higher proportion of maximum temperature variance through spring than does the model using SAM or the tropical TPI (Fig. 6 d-e). The percent variance explained is much higher in September (about 80%), before dropping to around 55% in October-November. The decrease in the percent variance explained appears to be primarily associated with how strongly the westerly winds correlate with maximum temperature over southern Australia; strong positive relationship with westerly wind in September changes to insignificant or negative in October and November (Supp. Fig S7 a-c). There is also an increase in negative correlation between maximum temperatures and northerly winds in north-eastern Australia (Supp. Fig S7 d-e) that will partly offset the increasing positive relationship further south. These changing relationships between dynamical mechanisms and maximum temperature through spring are linked with the changing relationships with the circulation features (Supp. Table 1) through spring. Overall, however, the three dynamical heat mechanisms explain much of Australia's monthly spring maximum temperature variability.

Figure 7 summarises the relationship between Australian maximum temperatures, circulation features, dynamical heat mechanisms and climate drivers through the spring months. The correlation between the SEC and Australian maximum temperature is strongest in September and rapidly decreases through October and November, while simultaneously the correlations with the SWC and particularly the SAA increase. As expected from Fig. 2, the SEC and SWC are more closely linked with the extratropics. Linearly regressing out the SAM component from time series of the SWC and SEC reduces the correlation strength with Australian maximum temperature (Fig. 7a), particularly in September. Conversely, linearly removing the tropical TPI slightly increases the correlation between the cyclones and temperature, with the partial-correlation only weakening in November. As SAM is strongly related to the barotropic cyclones it is also strongly related to how temperature changes with the westerly wind. Linearly removing SAM from the westerly wind time series nearly halves the correlation with maximum temperature in

September, and weakens the correlation in October and November (Fig. 7b). Conversely, linearly removing the tropical TPI actually increases the correlation slightly with the westerly wind in September and October, but decreases the correlation in November.

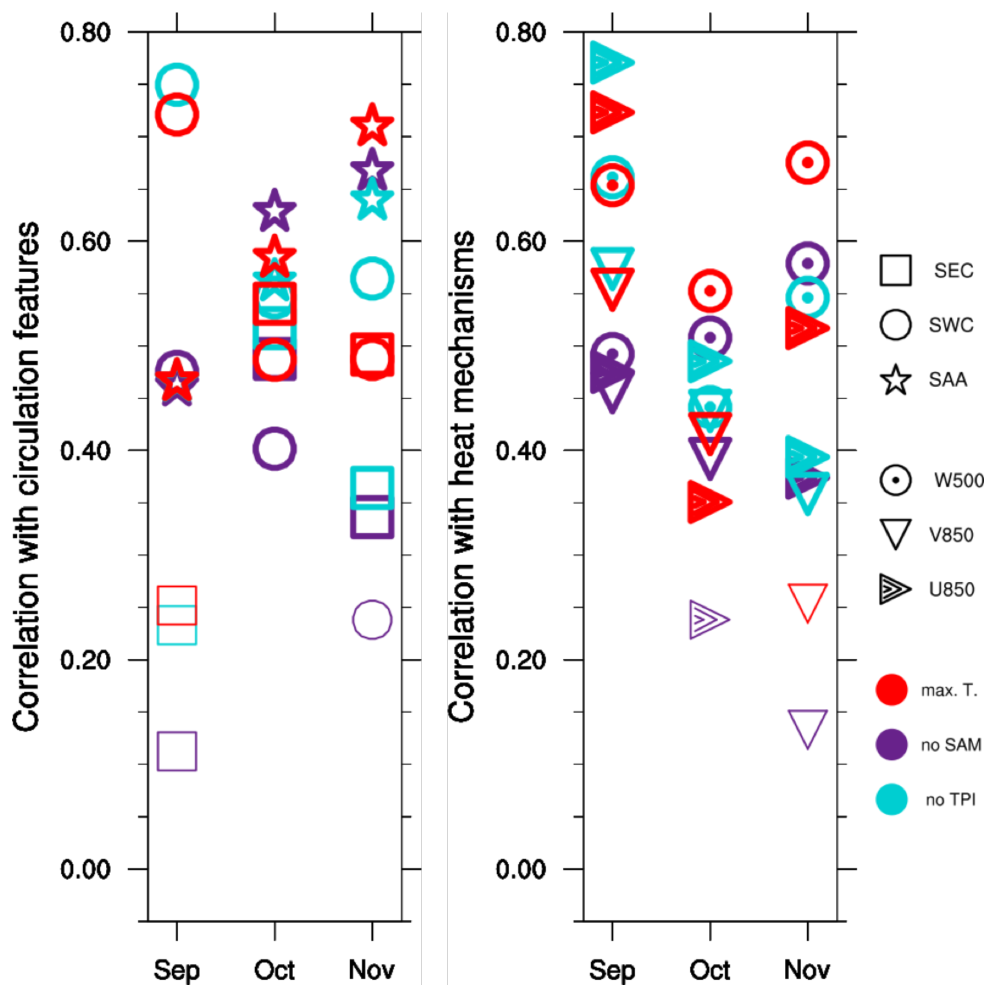

Figure 7. Correlations between Australian area-averaged maximum temperature (red) between key atmospheric circulation features (left figure) and dynamical heat mechanisms (right figure) for September, October and November. The purple and turquoise show partial correlations of the same, but with SAM and the tropical TPI linearly removed. Bold lines show the correlation was statistically significant at the 95% confidence level using a Student's t-test with 39 samples.

https://doi.org/10.5194/wcd-2021-63
Preprint. Discussion started: 4 October 2021

The relationships with northerly wind and sinking motion and Australian-averaged maximum temperature do not change as dramatically with the removal of SAM or the TPI. Northerly wind is not strongly influenced by the tropics or extratropics in September or October, but the correlation strengthens and weakens in November with the removal of the TPI and SAM, respectively. While removing SAM and TPI from the SAA had relatively little influence on the correlation with Australian maximum temperatures, removing SAM from sinking motion in September and both TPI and SAM in October and November reduced the correlation. Overall, it appears that the heat mechanisms associated with high maximum temperatures in spring are influenced differently by the different influence of the extratropics and tropics on the local atmospheric circulation features through spring.

7. Discussion and conclusions

The sources of the atmospheric circulation pattern associated with high monthly-maximum temperatures in Australia appear to change from primarily extratropical in early spring to tropical forcing in late spring. Examination of three dynamical heat mechanisms (low-level winds broken into westerly and northerly components, and mid-tropospheric sinking motion) indicates that this shift may be due to a change in how heat develops. In early spring, the low-level wind plays a greater role in maximum temperatures, advecting relatively warmer air from the oceans over the cold land-mass. This wind correlates strongly with the extratropics (here, SAM) as SAM projects strongly onto the southwest and southeast cyclones that direct a lot of the low-level flow around Australia. Conversely, the atmospheric circulation associated with the TPI (x-1) acts to counter the low-level flow that drives higher temperatures. Thus, in early spring we have a closer association with heat production and the extratropics. By late spring, the circulation patterns associated with high temperature have changed and the wind does not correlate as strongly. As such adiabatic sinking over subtropical Australia has a proportionally stronger correlation with high temperatures. Both SAM and TPI (x-1) regressions show sinking motion in the subtropics through spring, but it is the TPI that better matches the sinking motion over eastern Australia in November. Hence, the apparent change from extratropical to tropical forcing in the circulation pattern is because the tropics promotes more of the heat developing

https://doi.org/10.5194/wcd-2021-63
Preprint. Discussion started: 4 October 2021

mechanisms later in spring. However, much of the atmospheric patterns associated with heat through spring are explained by neither the tropical TPI nor SAM,

The subtropical jet appears to play a greater role in Australian spring heat by acting as a wave guide (Hoskins and Ambrizzi, 1993) that directs quasi-stationary Rossby waves toward Australia, rather than as a block that limits direct propagation of Rossby waves from the tropical Indian Ocean to the southern hemisphere extratropics (e.g. Simpkins et al., 2014; Li et al., 2015 a,b). While wave activity flux only appears to propagate directly out of the tropical Indian Ocean later in spring, this analysis does not suggest that the tropical Indian Ocean is not a wave source in early spring. Indeed, the results are broadly consistent with IOD-forced wave trains identified in the literature (Cai et al., 2011; McIntosh and Hendon, 2018; Wang et al., 2019). In particular, the secondary wave source in the high latitudes of the Indian Ocean proposed by McIntosh and Hendon (2018) may be key for promoting the TPI-forced atmospheric circulation in early spring, though this is beyond the scope of this study to confirm. As the subtropical jet did not act as a barrier preventing the tropical Indian Ocean's influence on Australia's maximum temperature, we argue instead that the apparent change in forcing through spring was more related to the origins of three of the dynamical heat mechanisms behind that heat. Consistent with this idea, wave activity flux calculated by first regressing 200Z onto the three dynamical heat mechanisms (Sup. Fig. 8) also has changing extratropical or tropical forcing through spring, that then propagates along the jet wave guide toward Australia.

Area-averaged low-level wind and vertical motion were used to understand how the atmospheric circulation relates to Australia-wide maximum temperatures, but do not form a complete picture of spring temperature development in Australia. Statistical models using these mechanisms explain much, but not all, of the maximum temperature variance over Australia. Further, it was not always clear how the atmospheric circulation features influenced those heat mechanisms. In particular, the southern Australian anticyclone and 500hPa subtropical-Australian sinking motion, while important for heat, appear to be largely uncorrelated with the other circulation features and mechanisms. Greater insight into how remote forcing of the atmospheric circulation results in high Australian temperatures could be gained by including other heat mechanisms in future analyses, including: insolation (Lim

https://doi.org/10.5194/wcd-2021-63
Preprint. Discussion started: 4 October 2021

et al., 2019b), land-surface feedbacks linked to antecedent moisture (e.g. Arblaster et al., 2014; Hirsch and King, 2020), and changes to synoptic weather systems (Cai et al., 2011; Hauser et al., 2020). How each of these mechanisms relates to the others, and geographic changes across Australia should also be considered. The combination of poleward advection of adiabatically warmed air after it descended anticyclonically over the Tasman Sea has been identified as a key mechanism for summer heatwaves in southeast Australia (e.g. Quinting and Reeder, 2017). This combination of mechanisms may generate heat through spring, particularly in the east and in November. The connection with rising motion over southern Australia has also not been examined, and may indicate the importance of air being diabatically warmed in association with storminess just to Australia's south, before advecting and descending toward Australia. While the three heat dynamical heat mechanisms were simple, the complex relationships between all of the mechanisms meant that the three used in this analysis were broadly representative of a large portion of how heat develops through spring.

We used the TPI to represent tropical variability relevant to Australia's maximum temperature, but other indices or drivers may highlight different Rossby wave pathways or heat mechanisms. Reconstructing Australian maximum temperature time series with more commonly used indices for the IOD and ENSO did not change the effectiveness of the statistical models overall (Supp. Fig. 4). However, it did suggest that the IOD had greater influence on Australia's maximum temperature in early spring than does ENSO, consistent with the seasonal-length studies of (Jones and Trewin, 2000; Saji et al., 2005). As such, we may expect different monthly Rossby wave pathways to Australia associate with the IOD in early spring, giving greater influence from the tropical Indian Ocean at this time. The MJO generates Rossby wave trains from the western Pacific that promote low minimum temperatures in Australia during winter (Wang and Hendon, 2020) and from the tropical Indian Ocean to promote high maximum temperatures in Australia in spring (personal communication: Wang and Hendon, 2021). The positive phase of the IOD suppresses MJO activity across the Indian Ocean (Wilson et al., 2013), possibly restricting the MJO's influence on Australia's maximum temperature at such times. However, MJO activity in the tropical Indian Ocean has recently been found to counter the wetting influence of La Niña during spring (Lim et al., 2021b). As such the MJO may be an important factor for spring

https://doi.org/10.5194/wcd-2021-63
Preprint. Discussion started: 4 October 2021

Weather and Climate Dynamics Discussions
Open Access
EGU

maximum temperatures when the tropical SSTs are not otherwise conducive for high temperatures, but is beyond the scope of this study.

As the trend toward higher Australian spring temperatures is projected to continue into the future a better understanding of what drives maximum temperatures over the months of spring is critical for better prediction and better preparation to adapt to a warming climate. A combination of extreme values in remote drivers of variability, including extreme positive IOD, central-Pacific El Niño, and sustained negative SAM associated with very strong sudden stratospheric warming, exacerbated already dry and hot conditions in spring 2019 to promote one of Australia's deadliest fire seasons (Watterson, 2020; Lim et al., 2021a; Abram et al., 2021, Marshall et al. 2021). Further, projected trends toward positive IOD (Cai et al., 2014; Abram et al., 2020) or toward negative TPI (Timbal and Hendon, 2011) may contribute to higher maximum temperatures in the future, particularly in later spring when the tropics exert greater influence on Australia's dynamical heat mechanisms. As we have shown just how different the atmospheric circulation and heat mechanisms can be through a season in Australia, other regions and seasons could also benefit from similar analysis, particular as the world continues to warm (e.g. Collins, et al., 2013).

Code and data availability

The code for analysis is available from the corresponding author on request. ERA5-reanalysis data are available from Copernicus Climate Change Service at https://www.ecmwf.int/en/forecasts/datasets/reanalysis-datasets/era5. AWAP data is available from the Australian Bureau of Meteorology.

Author contribution

R.M.C produced the figures and wrote the initial draft manuscript. All authors contributed to analysis and editing of the manuscript.

https://doi.org/10.5194/wcd-2021-63
Preprint. Discussion started: 4 October 2021

Competing interests

The authors declare that there are no conflicts of interests.

Acknowledgements

This research was supported by the Australian Research Council (ARC) Centre of Excellence for Climate Extremes (CE170100023). R.M. was also supported by an Australian Government Research Training Program (RTP) Scholarship and a Bureau of Meteorology PhD Top-up scholarship. J.M.A. was partially supported by the Regional and Global Model Analysis component of the Earth and Environmental System Modeling Program of the US Department of Energy's Office of Biological & Environmental Research via National Science Foundation IA 1947282. PH was supported by funding the Earth Systems and Climate Change Hub of the Australian Government's National Environmental Science Program (NESP). This research was undertaken at the NCI National Facility in Canberra, Australia, which is supported by the Australian Commonwealth Government. The NCAR Command Language (NCL; http://www.ncl.ucar.edu) version 6.4.0 was used for data analysis and visualization of the results. We thank G. Wang for his assistance writing code for analysis, Z. Gillett, E-P Lim, and H. Hendon for their insights into the data. The authors thank T. Turkington for supplying the tropical tripole index dataset. We thank H. Hendon and A. Marshall for their constructive feedback on the manuscript.

References

Abram, N. J., Wright, N. M., Ellis, B., Dixon, B. C., Wurtzel, J. B., England, M. H., Ummenhofer, C. C., Philibosian, B., Cahyarini, S. Y., Yu, T.-L., Shen, C.-C., Cheng, H., Edwards, R. L., and Heslop, D. (2020). Coupling of Indo-Pacific climate variability over the last millennium. *Nature*, *579*(7799), 385–392. https://doi.org/10.1038/s41586-020-2084-4

Abram, N. J., Henley, B. J., Sen Gupta, A., Lippmann, T. J. R., Clarke, H., Dowdy, A. J., Sharples, J. J., Nolan, R. H., Zhang, T., Wooster, M. J., Wurtzel, J. B., Meissner, K. J., Pitman, A. J., Ukkola, A. M., Murphy, B. P., Tapper, N. J., and Boer, M. M. (2021). Connections of climate change and variability to large and extreme forest fires in

https://doi.org/10.5194/wcd-2021-63
Preprint. Discussion started: 4 October 2021

Weather and Climate Dynamics Discussions
Open Access
EGU

southeast Australia. *Communications Earth and Environment*, *2*(1), 8. https://doi.org/10.1038/s43247-020-00065-8

Alexander, L. V., and Arblaster, J. M. (2009). Assessing trends in observed and modelled climate extremes over Australia in relation to future projections. *International Journal of Climatology*, *29*(3), 417–435. https://doi.org/10.1002/joc.1730

Arblaster, J., Lim, E.-P., Hendon, H., Trewin, B., Wheeler, M., Liu, G., and Braganza, K. (2014). UNDERSTANDING AUSTRALIA'S HOTTEST SEPTEMBER ON RECORD. *Bulletin of the American Meteorological Society*, *95*(9), S37–S41.

Bals-Elsholz, T. M., Atallah, E. H., Bosart, L. F., Wasula, T. A., Cempa, M. J., and Lupo, A. R. (2001). The Wintertime Southern Hemisphere Split Jet: Structure, Variability, and Evolution. *JOURNAL OF CLIMATE*, *14*, 25.

Barnes, E. A., and Hartmann, D. L. (2012). Detection of Rossby wave breaking and its response to shifts of the midlatitude jet with climate change: WAVE BREAKING AND CLIMATE CHANGE. *Journal of Geophysical Research: Atmospheres*, *117*(D9), n/a-n/a. https://doi.org/10.1029/2012JD017469

Boschat, G., Pezza, A., Simmonds, I., Perkins, S., Cowan, T., and Purich, A. (2015). Large scale and sub-regional connections in the lead up to summer heat wave and extreme rainfall events in eastern Australia. *Climate Dynamics*, *44*(7–8), 1823–1840. https://doi.org/10.1007/s00382-014-2214-5

Cai, W., van Rensch, P., Cowan T., and Hendon H. H., 2011a. 'Teleconnection Pathways of ENSO and the IOD and the Mechanisms for Impacts on Australian Rainfall'. *Journal of Climate* 24 (15): 3910–23. https://doi.org/10.1175/2011JCLI4129.1.

Cai, W., Santoso, A., Wang, G., Weller, E., Wu, L., Ashok, K., Masumoto, Y., and Yamagata, T. (2014). Increased frequency of extreme Indian Ocean Dipole events due to greenhouse warming. *Nature*, *510*(7504), 254–258. https://doi.org/10.1038/nature13327

Ceppi, P., and Hartmann, D. L. (2013). On the Speed of the Eddy-Driven Jet and the Width of the Hadley Cell in the Southern Hemisphere. *Journal of Climate*, *26*(10), 3450–3465. https://doi.org/10.1175/JCLI-D-12-00414.1

Collins, M., Knutti, R., Arblaster, J., Dufresne, J.-L., Fichefet, T., Friedlingstein, P., Gao, X., Gutowski, W. J., Johns, T., Krinner, G., Shongwe, M., Tebaldi, C., Weaver, A. J., Wehner, M. F., Allen, M. R., Andrews, T., Beyerle, U., Bitz, C. M., Bony, S., and Booth,

https://doi.org/10.5194/wcd-2021-63
Preprint. Discussion started: 4 October 2021

B. B. B. (2013). Long-term Climate Change: Projections, Commitments and Irreversibility. *Climate Change 2013 - The Physical Science Basis: Contribution of Working Group I to the Fifth Assessment Report of the Intergovernmental Panel on Climate Change*, 1029–1136.

Cullen, B. R., Johnson, I. R., Eckard, R. J., Lodge, G. M., Walker, R. G., Rawnsley, R. P., and McCaskill, M. R. (2009). Climate change effects on pasture systems in south-eastern Australia. *Crop and Pasture Science*, *60*(10), 933. https://doi.org/10.1071/CP09019

Dee, D. P., Uppala, S. M., Simmons, A. J., Berrisford, P., Poli, P., Kobayashi, S., Andrae, U., Balmaseda, M. A., Balsamo, G., Bauer, P., Bechtold, P., Beljaars, A. C. M., van de Berg, L., Bidlot, J., Bormann, N., Delsol, C., Dragani, R., Fuentes, M., Geer, A. J., … Vitart, F. (2011). The ERA-Interim reanalysis: Configuration and performance of the data assimilation system. *Quarterly Journal of the Royal Meteorological Society*, *137*(656), 553–597. https://doi.org/10.1002/qj.828

Dowdy, A. J. (2018). Climatological Variability of Fire Weather in Australia. *Journal of Applied Meteorology and Climatology*, *57*(2), 221–234. https://doi.org/10.1175/JAMC-D-17-0167.1

Fogt, R. L., and Marshall, G. J. (2020). The Southern Annular Mode: Variability, trends, and climate impacts across the Southern Hemisphere. *WIREs Climate Change*, *11*(4). https://doi.org/10.1002/wcc.652

Gallant, A. J. E., and Lewis, S. C. (2016). Stochastic and anthropogenic influences on repeated record-breaking temperature extremes in Australian spring of 2013 and 2014: CAUSES OF REPEATED TEMPERATURE RECORDS. *Geophysical Research Letters*, *43*(5), 2182–2191. https://doi.org/10.1002/2016GL067740

Gibson, P. B., Pitman, A. J., Lorenz, R., and Perkins-Kirkpatrick, S. E. (2017). The Role of Circulation and Land Surface Conditions in Current and Future Australian Heat Waves. *Journal of Climate*, *30*(24), 9933–9948. https://doi.org/10.1175/JCLI-D-17-0265.1

Gillett, Z. E., Hendon, H. H., Arblaster, J. M., and Lim, E.-P. (2021). Tropical and Extratropical Influences on the Variability of the Southern Hemisphere Wintertime Subtropical Jet. *Journal of Climate*, *34*(10), 4009–4022. https://doi.org/10.1175/JCLI-D-20-0460.1

Gong, D., and Wang, S. (1999). Definition of Antarctic Oscillation index. *Geophysical Research Letters*, *26*(4), 459–462. https://doi.org/10.1029/1999GL900003

https://doi.org/10.5194/wcd-2021-63
Preprint. Discussion started: 4 October 2021

Harris S., and Lucas, C. (2019). Understanding the variability of Australian fire weather between 1973 and 2017. *PLoS ONE, 14*, e0222328.

Hauser, S., Grams, C. M., Reeder, M. J., McGregor, S., Fink, A. H., and Quinting, J. F. (2020). A weather system perspective on winter–spring rainfall variability in southeastern Australia during El Niño. *Quarterly Journal of the Royal Meteorological Society*, qj.3808. https://doi.org/10.1002/qj.3808

Hendon, H. H., Lim, E.-P., and Nguyen, H. (2014). Seasonal Variations of Subtropical Precipitation Associated with the Southern Annular Mode. *Journal of Climate*, *27*(9), 3446–3460. https://doi.org/10.1175/JCLI-D-13-00550.1

Hendon, H. H., Thompson, D. W. J., and Wheeler, M. C. (2007). Australian Rainfall and Surface Temperature Variations Associated with the Southern Hemisphere Annular Mode. *Journal of Climate*, *20*(11), 2452–2467. https://doi.org/10.1175/JCLI4134.1

Hersbach, H., Bell, B., Berrisford, P., Hirahara, S., Horányi, A., Muñoz-Sabater, J., Nicolas, J., Peubey, C., Radu, R., Schepers, D., Simmons, A., Soci, C., Abdalla, S., Abellan, X., Balsamo, G., Bechtold, P., Biavati, G., Bidlot, J., Bonavita, M., … Thépaut, J. (2020). The ERA5 global reanalysis. *Quarterly Journal of the Royal Meteorological Society*, *146*(730), 1999–2049. https://doi.org/10.1002/qj.3803

Hirsch, A. L., & King, M. J. (2020). Atmospheric and Land Surface Contributions to Heatwaves: An Australian Perspective. *Journal of Geophysical Research: Atmospheres*, *125*(17). https://doi.org/10.1029/2020JD033223

Holgate, C. M., Van Dijk, A. I. J. M., Evans, J. P., and Pitman, A. J. (2020). Local and Remote Drivers of Southeast Australian Drought. *Geophysical Research Letters*, *47*(18). https://doi.org/10.1029/2020GL090238

Hope, P., Lim, E.-P., Wang, G., Hendon, H. H., and Arblaster, J. M. (2015). Contributors to the Record High Temperatures Across Australia in Late Spring 2014. *Bulletin of the American Meteorological Society*, *96*(12), S149–S153.

Hope, P., Wang, G., Lim, E.-P., Hendon, H. H., and Arblaster, J. M. (2016). WHAT CAUSED THE RECORD-BREAKING HEAT ACROSS AUSTRALIA IN OCTOBER 2015? [in “Explaining Extreme Events of 2015 from a Climate Perspective”]. *Bulletin of the American Meteorological Society*, *96*(12 (suppl)), S1–S172. https://doi.org/10.1175/BAMS-D-15-00157.1

https://doi.org/10.5194/wcd-2021-63
Preprint. Discussion started: 4 October 2021

Hope, P., and Watterson, I. (2018). Persistence of cool conditions after heavy rain in Australia. *Journal of Southern Hemisphere Earth System Science*, *68*(1). https://doi.org/10.22499/3.6801.004

Hoskins, B. J., & Karoly, D. J. (1981). The Steady Linear Response of a Spherical Atmosphere to Thermal and Orographic Forcing. Journal of the Atmospheric Sciences. https://doi.org/10.1175/1520-0469(1981)038<1179:TSLROA>2.0.CO;2

Hoskins B.J., Ambrizzi T. (1993) Rossby wave propagation on a realistic longitudinally varying flow. J Atmos Sci 50:1661–1671

Huang, B., Peter W. Thorne, et. al, 2017: Extended Reconstructed Sea Surface Temperature version 5 (ERSSTv5), Upgrades, validations, and intercomparisons. J. Climate, doi: 10.1175/JCLI-D-16-0836.1

Hurrell, J., Meehl, G. A., Bader, D., Delworth, T. L., Kirtman, B., and Wielicki, B. (2009). A Unified Modeling Approach to Climate System Prediction. *Bulletin of the American Meteorological Society*, *90*(12), 1819–1832. https://doi.org/10.1175/2009BAMS2752.1

Japan Meteorological Agency/Japan (2013), JRA-55: Japanese 55-year Reanalysis, Daily 3-Hourly and 6-Hourly Data, https://doi.org/10.5065/D6HH6H41, Research Data Archive at the National Center for Atmospheric Research, Computational and Information Systems Laboratory, Boulder, Colo. (Updated monthly.) Accessed December 2020.

Jarvis, C., Darbyshire, R., Goodwin, I., Barlow, E. W. R., and Eckard, R. (2019). Advancement of winegrape maturity continuing for winegrowing regions in Australia with variable evidence of compression of the harvest period: Advancement of winegrape maturity. *Australian Journal of Grape and Wine Research*, *25*(1), 101–108. https://doi.org/10.1111/ajgw.12373

Jones, D., and Trewin, B. C. (2000). On the relationships between the El Niño-Southern Oscillation and Australian land surface temperature. *Int. J. Climatol.*, 23.

Jones, D., Wang, W., and Fawcett, R. (2009). High-quality spatial climate data-sets for Australia. *Australian Meteorological and Oceanographic Journal*, *58*(04), 233–248. https://doi.org/10.22499/2.5804.003

https://doi.org/10.5194/wcd-2021-63
Preprint. Discussion started: 4 October 2021

Koch, P., Wernli, H., and Davies, H. C. (2006). An event-based jet-stream climatology and typology. *International Journal of Climatology*, *26*(3), 283–301. https://doi.org/10.1002/joc.1255

L'Heureux, M. L., and Thompson, D. W. J. (2006). Observed Relationships between the El Niño–Southern Oscillation and the Extratropical Zonal-Mean Circulation. *Journal of Climate*, *19*(2), 276–287. https://doi.org/10.1175/JCLI3617.1

Li, X., Gerber, E. P., Holland, D. M., and Yoo, C. (2015). A Rossby Wave Bridge from the Tropical Atlantic to West Antarctica. *Journal of Climate*, *28*(6), 2256–2273. https://doi.org/10.1175/JCLI-D-14-00450.1

Li, X., Holland, D. M., Gerber, E. P., and Yoo, C. (2015). Rossby Waves Mediate Impacts of Tropical Oceans on West Antarctic Atmospheric Circulation in Austral Winter. *Journal of Climate*, *28*(20), 8151–8164. https://doi.org/10.1175/JCLI-D-15-0113.1

Lim, E. P., Hendon, H. H., Arblaster, J. M., Chung, C., Moise, A. F., Hope, P., Young, G., and Zhao, M. (2016). Interaction of the recent 50 year SST trend and La Niña 2010: amplification of the Southern Annular Mode and Australian springtime rainfall. Climate Dynamics, 47(7–8), 2273–2291. https://doi.org/10.1007/s00382-015-2963-

Lim, E. -P., Hendon, H. H., and Thompson, D. W. J. (2018). Seasonal Evolution of Stratosphere-Troposphere Coupling in the Southern Hemisphere and Implications for the Predictability of Surface Climate. *Journal of Geophysical Research: Atmospheres*, *123*(21), 12,002-12,016. https://doi.org/10.1029/2018JD029321

Lim, E.-P., Hendon, H., Hope, P., Chung, C., Delage, F., and McPhaden, M. J. (2019a). Continuation of tropical Pacific Ocean temperature trend may weaken extreme El Niño and its linkage to the Southern Annular Mode. *Scientific Reports*, 15. https://doi.org/10.1038/s41598-019-53371-3

Lim, E.-P., Hendon, H. H., Boschat, G., Hudson, D., Thompson, D. W. J., Dowdy, A. J., and Arblaster, J. M. (2019b). Australian hot and dry extremes induced by weakenings of the stratospheric polar vortex. *Nature Geoscience*, *12*(11), 896–901. https://doi.org/10.1038/s41561-019-0456-x

Lim, E.-P., Hendon, H. H., Butler, A. H., Thompson, D. W. J., Lawrence, Z. D., Scaife, A. A., Shepherd, T. G., Polichtchouk, I., Nakamura, H., Kobayashi, C., Comer, R., Coy, L., Dowdy, A., Garreaud, R. D., Newman, P. A., and Wang, G. (2021a). The 2019 Southern Hemisphere Stratospheric Polar Vortex Weakening and Its Impacts. *Bulletin*

https://doi.org/10.5194/wcd-2021-63
Preprint. Discussion started: 4 October 2021

of the American Meteorological Society, *102*(6), E1150–E1171. https://doi.org/10.1175/BAMS-D-20-0112.1

Lim, E.-P., Hudson, D., Wheeler, M. C., Marshall, A. G., King, A., Zhu, H., Hendon, H. H., de Burgh-Day, C., Trewin, B., Griffiths, M., Ramchurn, A., & Young, G. (2021b). Why Australia was not wet during spring 2020 despite La Niña. *Scientific Reports*, *11*(1), 18423. https://doi.org/10.1038/s41598-021-97690-w

Liu, Z., & Alexander, M. (2007). Atmospheric bridge, oceanic tunnel, and global climatic teleconnections. *Reviews of Geophysics*, *45*(2), RG2005. https://doi.org/10.1029/2005RG000172

Maher, P., and Sherwood, S. C. (2014). Disentangling the Multiple Sources of Large-Scale Variability in Australian Wintertime Precipitation. *Journal of Climate*, *27*(17), 6377–6392. https://doi.org/10.1175/JCLI-D-13-00659.1

Marshall, G. J. (2003). Trends in the Southern Annular Mode from Observations and Reanalyses. *JOURNAL OF CLIMATE*, *16*, 10.

Marshall, A. G., Hudson, D., Wheeler, M. C., Hendon, H. H., and Alves, O. (2012). Simulation and prediction of the Southern Annular Mode and its influence on Australian intra-seasonal climate in POAMA. *Climate Dynamics*, *38*(11–12), 2483–2502. https://doi.org/10.1007/s00382-011-1140-z

Marshall, A., Hudson, D., Wheeler, M., Alves, O., Hendon, H., Pook, M., and Risbey, J. (2014). Intra-seasonal drivers of extreme heat over Australia in observations and POAMA-2. *Climate Dynamics*, *43*(7–8), 1915–1937. https://doi.org/10.1007/s00382-013-2016-1

Marshall, A. G., Gregory, P. A., de Burgh-Day, C. O., and Griffiths, M. (2021). Subseasonal drivers of extreme fire weather in Australia and its prediction in ACCESS-S1 during spring and summer. *Climate Dynamics*, accepted.

McIntosh, P. C., and Hendon, H. H. (2018). Understanding Rossby wave trains forced by the Indian Ocean Dipole. *Climate Dynamics*, *50*(7–8), 2783–2798. https://doi.org/10.1007/s00382-017-3771-1

McKay, R. C., Arblaster, J. M., Hope, P., and Lim, E.-P. (2021). Exploring atmospheric circulation leading to three anomalous Australian spring heat events. *Climate Dynamics*, *56*(7–8), 2181–2198. https://doi.org/10.1007/s00382-020-05580-0

Meehl, G. A., Richter, J. H., Teng, H., Capotondi, A., Cobb, K., Doblas-Reyes, F., Donat, M. G., England, M. H., Fyfe, J. C., Han, W., Kim, H., Kirtman, B. P., Kushnir, Y., Lovenduski, N.

https://doi.org/10.5194/wcd-2021-63
Preprint. Discussion started: 4 October 2021

S., Mann, M. E., Merryfield, W. J., Nieves, V., Pegion, K., Rosenbloom, N., … Xie, S.-P. (2021). Initialized Earth System prediction from subseasonal to decadal timescales. *Nature Reviews Earth & Environment*. https://doi.org/10.1038/s43017-021-00155-x

Meyers, G., McIntosh, P., Pigot, L., and Pook, M. (2007). The Years of El Niño, La Niña, and Interactions with the Tropical Indian Ocean. *Journal of Climate*, *20*(13), 2872–2880. https://doi.org/10.1175/JCLI4152.1

Min, S.-K., Cai, W., and Whetton, P. (2013). Influence of climate variability on seasonal extremes over Australia: SEASONAL EXTREMES OVER AUSTRALIA. *Journal of Geophysical Research: Atmospheres*, *118*(2), 643–654. https://doi.org/10.1002/jgrd.50164

Nairn, J., and Fawcett, R. (2014). The Excess Heat Factor: A Metric for Heatwave Intensity and Its Use in Classifying Heatwave Severity. *International Journal of Environmental Research and Public Health*, *12*(1), 227–253. https://doi.org/10.3390/ijerph120100227

Nicholls, N., 1989. Sea surface temperature and Australian winter rainfall. J. Clim. 2, 965–973.

Pepler, A., Timbal, B., Rakich, C., and Coutts-Smith, A. (2014). Indian Ocean Dipole Overrides ENSO's Influence on Cool Season Rainfall across the Eastern Seaboard of Australia. *Journal of Climate*, *27*(10), 3816–3826. https://doi.org/10.1175/JCLI-D-13-00554.1

Pepler, A., Dowdy, A. J., van Rensch, P., Rudeva, I., Catto, J. L., and Hope, P. (2020). The contributions of fronts, lows and thunderstorms to southern Australian rainfall. *Climate Dynamics*. https://doi.org/10.1007/s00382-020-05338-8

Pfahl, S., Schwierz, C., Croci-Maspoli, M., Grams, C. M., and Wernli, H. (2015). Importance of latent heat release in ascending air streams for atmospheric blocking. *Nature Geoscience*, *8*(8), 610–614. https://doi.org/10.1038/ngeo2487

Power, S., Tseitkin, F., Torok, S., Lavery, B., Dahni, R., and McAvaney, B. (1998). Australian temperature, Australian rainfall and the Southern Oscillation, 1910-1992: coherent variability and recent changes. Australian Meteorological Magazine, 47, 85–101.

Quinting, J. F., and Reeder, M. J. (2017). Southeastern Australian Heat Waves from a Trajectory Viewpoint. *Monthly Weather Review*, *145*(10), 4109–4125. https://doi.org/10.1175/MWR-D-17-0165.1

Risbey, J. S., Pook, M. J., McIntosh, P. C., Wheeler, M. C., and Hendon, H. H. (2009a). On the Remote Drivers of Rainfall Variability in Australia. *Monthly Weather Review*, *137*(10), 3233–3253. https://doi.org/10.1175/2009MWR2861.1

Risbey, J. S., Pook, M. J., McIntosh, P. C., Ummenhofer, C. C., and Meyers, G. (2009b). Characteristics and variability of synoptic features associated with cool season rainfall in southeastern Australia. *International Journal of Climatology*, *29*(11), 1595–1613. https://doi.org/10.1002/joc.1775

Saji, N. H., Goswami, B. N., Vinayachandran, P. N., and Yamagata, T. (1999). A dipole mode in the tropical Indian Ocean. *Nature*, *401*(6751), 360–363. https://doi.org/10.1038/43854

Saji, N. H., Ambrizzi, T., and Ferraz, S. E. T. (2005). Indian Ocean Dipole mode events and austral surface air temperature anomalies. *Dynamics of Atmospheres and Oceans*, *39*(1–2), 87–101. https://doi.org/10.1016/j.dynatmoce.2004.10.015

Simpkins, G. R., McGregor, S., Taschetto, A. S., Ciasto, L. M., and England, M. H. (2014). Tropical Connections to Climatic Change in the Extratropical Southern Hemisphere: The Role of Atlantic SST Trends. *Journal of Climate*, *27*(13), 4923–4936. https://doi.org/10.1175/JCLI-D-13-00615.1

Simmonds, I. (1998). Seasonal and regional responses to changes in Australian soil moisture conditions. *Int. J. Climatol.*, 35.

Student, (1908). The probable error of a mean, *Biometrika*, 6, 1–25.

Suarez-Gutierrez, L., Müller, W. A., Li, C., and Marotzke, J. (2020). Dynamical and thermodynamical drivers of variability in European summer heat extremes. *Climate Dynamics*, *54*(9–10), 4351–4366. https://doi.org/10.1007/s00382-020-05233-2

Takaya, K., and Nakamura, H. (2001). A Formulation of a Phase-Independent Wave-Activity Flux for Stationary and Migratory Quasigeostrophic Eddies on a Zonally Varying Basic Flow. *JOURNAL OF THE ATMOSPHERIC SCIENCES*, *58*, 20.

Taylor, C., Cullen, B., D'Occhio, M., Rickards, L., and Eckard, R. (2018). Trends in wheat yields under representative climate futures: Implications for climate adaptation. *Agricultural Systems*, *164*, 1–10. https://doi.org/10.1016/j.agsy.2017.12.007

Thompson, D. W. J., and Wallace, J. M. (2000). Annular Modes in the Extratropical Circulation. Part I: Month-to-Month Variability. *JOURNAL OF CLIMATE*, *13*, 17.

https://doi.org/10.5194/wcd-2021-63
Preprint. Discussion started: 4 October 2021

Timbal, B., Power, S., Colman, R., Viviand, J., & Lirola, S. (2002). Does Soil Moisture Influence Climate Variability and Predictability over Australia? Journal of Climate, 15(10), 1230–1238. https://doi.org/10.1175/1520-0442(2002)015<1230:dsmicv>2.0.co;2

Timbal, B., and Hendon, H. (2011). The role of tropical modes of variability in recent rainfall deficits across the Murray-Darling Basin: TROPICAL VARIABILITY AND RAINFALL DEFICIT IN THE MDB. *Water Resources Research*, *47*(12). https://doi.org/10.1029/2010WR009834

Ummenhofer, C. C., England, M. H., McIntosh, P. C., Meyers, G. A., Pook, M. J., Risbey, J. S., Gupta, A. S., and Taschetto, A. S. (2009). What causes southeast Australia's worst droughts? *Geophysical Research Letters*, *36*(4), L04706. https://doi.org/10.1029/2008GL036801

van Rensch, P., Arblaster, J., Gallant, A. J. E., Cai, W., Nicholls, N., and Durack, P. J. (2019). Mechanisms causing east Australian spring rainfall differences between three strong El Niño events. *Climate Dynamics*, *53*(5–6), 3641–3659. https://doi.org/10.1007/s00382-019-04732-1

Wang, G., and Hendon, H. H. (2020). Impacts of the Madden–Julian Oscillation on wintertime Australian minimum temperatures and Southern Hemisphere circulation. *Climate Dynamics*, *55*(11–12), 3087–3099. https://doi.org/10.1007/s00382-020-05432-x

Wang, G., Hendon, H. H., Arblaster, J. M., Lim, E.-P., Abhik, S., and van Rensch, P. (2019). Compounding tropical and stratospheric forcing of the record low Antarctic sea-ice in 2016. *Nature Communications*, *10*(1), 13. https://doi.org/10.1038/s41467-018-07689-7

Watterson, I. G. (2010). Relationships between southeastern Australian rainfall and sea surface temperatures examined using a climate model. *Journal of Geophysical Research*, *115*(D10), D10108. https://doi.org/10.1029/2009JD012120

Watterson, I. G. (2020). Australian Rainfall Anomalies in 2018–2019 Linked to Indo-Pacific Driver Indices Using ERA5 Reanalyses. *Journal of Geophysical Research: Atmospheres*, *125*(17). https://doi.org/10.1029/2020JD033041

Wheeler, M.C. and Hendon, H.H. 2004. An all-season real-time multivariate MJO index: Development of an index for monitoring and prediction. Monthly Weather Review, 132, 1917–1932

https://doi.org/10.5194/wcd-2021-63
Preprint. Discussion started: 4 October 2021

Wheeler, M. C., Hendon, H. H., Cleland, S., Meinke, H., and Donald, A. (2009). Impacts of the Madden–Julian Oscillation on Australian Rainfall and Circulation. *Journal of Climate*, *22*(6), 1482–1498. https://doi.org/10.1175/2008JCLI2595.1

White, C. J., Hudson, D., and Alves, O. (2014). ENSO, the IOD and the intraseasonal prediction of heat extremes across Australia using POAMA-2. *Climate Dynamics*, *43*(7–8), 1791–1810. https://doi.org/10.1007/s00382-013-2007-2

Wilson, E. A., Gordon, A. L., & Kim, D. (2013). Observations of the Madden Julian Oscillation during Indian Ocean Dipole events: IOD-MJO. *Journal of Geophysical Research: Atmospheres*, *118*(6), 2588–2599. https://doi.org/10.1002/jgrd.50241